American Mineralogist, Volume 84, pages 420–434, 1999

XAFS determination of the chemical form of lead in smelter-contaminated soils and mine tailings: Importance of adsorption processes

GUILLAUME MORIN,[1] JOHN D. OSTERGREN,[2] FARID JUILLOT,[1] PHILIPPE ILDEFONSE,[1] GEORGES CALAS,[1] AND GORDON E. BROWN JR.[2,3,*]

[1]Laboratoire de Minéralogie-Cristallographie, URA CNRS 09, Universités de Paris 6 et 7, 4 Place Jussieu, 75252 Paris Cedex 05, France

[2]Department of Geological and Environmental Sciences, Stanford University, Stanford, California 94305–2115, U.S.A.

[3]Stanford Synchrotron Radiation Laboratory, SLAC, Stanford, California 94309, U.S.A.

ABSTRACT

We investigated smelter-contaminated soils from Evin-Malmaison, Nord-Pas-de-Calais, France, and mine tailings from Leadville, Colorado, U.S.A. Bulk Pb concentrations range from 460 to 1900 ppm in the topsoils at Evin-Malmaison site and from 6000 to 10000 ppm in the tailings samples from the Leadville site. These concentrations necessarily raise human health and environmental concerns, but bioavailability and chemical lability of Pb in these materials vary dramatically and show little correlation with bulk concentrations. This study provides detailed information on the speciation of Pb in these materials. Emphasis is on the identification and characterization of poorly crystalline and/or fine-grained species, such as sorption complexes and poorly crystalline (co)precipitates, which are likely to control Pb bioavailability and mobility in these natural systems.

Because these samples are heterogeneous, multi-phase mixtures, a variety of bulk analytical methods were used including powder X-ray diffraction (XRD) and Rietveld refinement, scanning electron microscopy, electron probe microanalysis, synchrotron-based X-ray absorption, and micro-fluorescence spectroscopies. The synchrotron-based techniques enable identification of amorphous or nanocrystalline Pb-containing phases and the spatial distribution of Pb at the 25 μm scale.

These techniques, in conjunction with physical and chemical separation techniques, allowed identification and characterization of several species not amenable to detection by conventional microanalytical techniques. In the Evin-Malmaison samples, direct spectroscopic evidence for Pb sorbed to humic acids was found, as well as to both manganese and iron (oxyhydr)oxides. In the Leadville samples, variations in Pb speciation with pH are consistent with predictions based on simplified model system studies of adsorption processes; specifically, the carbonate-buffered tailings with near-neutral pH contain up to 50% of total Pb as adsorption complexes on iron (oxyhydr)oxides, whereas Pb speciation in sulfide-rich low pH samples is dominated by Pb-bearing jarosites with no evidence for adsorbed Pb in these latter samples.

INTRODUCTION

The bioavailability, toxicity, and mobility of toxic metals and metalloids are controlled by and can vary widely with speciation, i.e., the chemical form and characteristics of elements, including (1) coordination environment (number and types of ligands and more distant neighbors, metal-ligand and metal-second-neighbor distances); (2) oxidation state; (3) presence as an adsorption complex, precipitate, or solid solution; and (4) type(s) of phase with which they are associated (e.g., Davis et al. 1992, 1993; Gulson et al. 1994; Ruby et al. 1992). Whereas many metal species can be readily identified by conventional analytical techniques with micrometer-scale resolution, such as electron probe micro-analysis (EPMA) and scanning electron microscopy (SEM), these techniques are unable to identify or distinguish among the myriad of possible surface and other species occurring on the sub-micrometer scale, such as adsorbates and thin surface precipitates. Furthermore, speciation of contaminant elements may be altered under the ultra-high-vacuum (UHV) conditions required for these and other analytical techniques (X-ray photoelectron spectroscopy, XPS, and others), especially when water is present. Surface metal speciation in natural environments is, therefore, often evaluated by indirect methods, such as ''selective'' chemical extractions (e.g., Tessier et al. 1996; Kimball et al. 1995; Levy et al. 1992). Although valuable in their own right, these methods are naturally limited by their indirect

* E-mail: gordon@pangea.stanford.edu

0003–004X/99/0003–0420$05.00

approach, and full characterization of Pb species in natural systems ultimately requires direct and in situ analyses, using methods such as XAFS spectroscopy (e.g., Cotter-Howells et al. 1994; Manceau et al. 1996; O'Day et al. 1998; Ostergren et al., unpublished manuscript).

In the present paper, EXAFS studies of complex environmental materials (soils and mine-tailings) and simplified Pb-containing model compounds have been coupled with studies using XRD, SEM, EPMA, and chemical extractions. Because of the tendency of aqueous Pb ions to bind or sorb to the surfaces of natural solids—particularly iron and manganese oxides and oxyhydroxides and natural organic matter—comparisons of the Pb-EXAFS spectra of the soils and mine tailings with those of Pb sorbed to the surfaces of representative (oxyhydr)oxides and humic substances were also made. These comparisons were facilitated by the growing data base of EXAFS spectra of Pb sorbed to various oxide, (oxy)hydroxide, and aluminosilicate surfaces (e.g., Chilsholm-Brause et al. 1990; Roe et al. 1991; Manceau et al. 1992; Bargar et al. 1996, 1997a, 1997b, 1997c; Farquhar et al. 1997) and humic substances (Xia et al. 1997). The primary objective here is to characterize Pb species such as adsorbates and other sub-micrometer scale species, which are not amenable to direct and in situ analysis by non-synchrotron-based techniques.

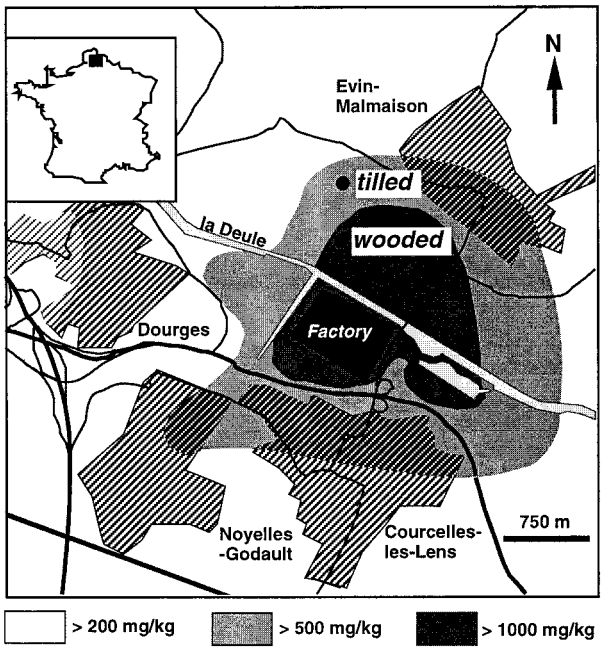

FIGURE 1. Geographic location of the smelter contaminated area studied. Contours of lead iso-concentrations at values of 200, 500, and 1000 ppm in the topsoil are shown. The location of the two profiles sampled are also labeled (data from Godin et al. 1985).

MATERIALS AND SAMPLE PREPARATION

Smelter-contaminated soils from Evin-Malmaison (Nord-Pas-de-Calais, France)

The smelter-impacted site studied is located in the largest producing Pb-Zn mining and processing region in Europe (Evin-Malmaison, Nord-Pas-de-Calais, France), and has been active for more than 100 years (Fig. 1). The emission of dust with high contents of Pb, Zn, and Cd has impacted agricultural fields used for farming and livestock breeding activities. Lead levels currently exceed 200 ppm in soils throughout a 40 km^2 area surrounding the central smelter. This site (no. 62.0030) is one of the 896 polluted French sites recognized in 1996 by the French Ministry of Environment (Ministère de l'Environnement 1996).

The two soils studied can be classified as pseudogley brown leached soils (Luvisol Redoxisol). The bedrock is Ostricourt clay-rich sands, overlain by a 60 to 150 cm thick clay-rich silt layer. Both soils are within the interval area of the phreatic sheet located at about 100 cm depth. The first profile, referred to as tilled soil hereafter, is located in an agricultural field, at about 1000 m NE from the smelter. This soil has a tilled horizon down to 30 cm depth due to farming. The second profile, referred to as wooded soil hereafter, is located at 500 m NE from the smelter in a wooded plot that has not been disrupted for about 50 years. Bulk Pb concentrations range up to 460 and 1900 ppm in the topsoil (0 to 5 cm) of the tilled and wooded soils respectively. Both soils were sampled over a large depth interval (120 cm for tilled soil and 100 cm for wooded soil). The topsoils from the two profiles differ in pH (7.5 and 6.5) and organic matter content (1.5 wt% tilled and 6.4 wt% for the wooded soil).

Bulk samples were first wet sieved at 200 μm, then at 50 μm. No detectable loss of Pb during the wet sieving was noted. The fraction smaller than 50 μm was allowed to settle for 16 hours in water columns to isolate the <2 μm fraction. This operation was repeated until the soil suspension was clear. The 2 to 50 μm, 50 to 200 μm, and >200 μm fractions contained particles of varying density and magnetic properties. Denser particles were separated from the bulk samples by settling in bromoform ($CHBr_3$, $d = 2.89$ g/cm^3) and were then washed with acetone and air-dried.

Chemical compositions of bulk samples and fine fractions (Table 1) were determined at the Centre de Recherches Petrographiques et Geochimiques (CRPG Nancy, France). Bulk samples were ground to fine powders (<30 μm) using an agate mortar and pestle. After fusion of each sample with $LiBO_2$ followed by HNO_3 dissolution, major (Si, Al, Fe, Ca, Na, K, Mn, Mg, P, and Ti) and trace (Pb, Zn, and Cd) elements were determined by ICP-emission and ICP-MS respectively.

Chemical treatments were performed on the fine fraction of each soil sample to help interpret EXAFS data. Exchangeable species were extracted by reacting 1g of the fine fraction with 100 mL of 0.5 *M* $CaCl_2$ at room temperature for 2 h. Two separate treatments were used to extract the fraction of Pb bound to organic matter from

TABLE 1. Chemical composition of Evin-Malmaison, France, soils and Leadville, Colorado, U.S.A., tailings samples

	Evin-Malmaison					Leadville	
	Tilled soil 0–5 cm		Wooded soil 0–5 cm			Hamms tailings <100 μm	Apache tailings <100 μm
	Bulk	<2 μm	Bulk	<2 μm			
Major and minor elements (wt%)							
SiO_2	76.70	44.85	71.75	44.5			
Al_2O_3	7.22	16.35	7.95	15.34	Al	0.56	0.54
Fe_2O_3	3.01	9.31	3.67	9.0	Fe	6.18	16.4
MnO	0.05	0.12	0.05	0.04	Mn	0.83	0.12
MgO	0.57	1.85	0.74	1.84	Mg	2.43	0.31
CaO	1.16	1.84	0.58	1.05	Ca	4.00	3.99
Na_2O	0.88	0.23	0.78	0.18	Na	0.03	0.03
K_2O	1.82	2.76	1.82	2.3	K	0.18	0.32
TiO_2	0.70	0.8	0.68	0.68	Ti	<0.01	<0.01
P_2O_5	0.16	0.39	0.15	0.39	P	0.16	0.12
L.O.I.*	6.61	20.94	10.39	23.92			
Totals	98.87	99.44	98.56	99.24			
Trace elements (mg/kg)							
Pb	465	1997	1910	4288		8520	8330
Zn	571	2746	1380	4391		>10000	7970
Cd	9.2	30.4	25.2	64.4		97	31
pH	7.5		6.5			6.8	2.7
T.O.C. (wt%)	1.5		6.4			<0.01	0.27

* L.O.I. = loss on ignition.
† T.O.C. = total organic carbon.

the fine fraction not associated with organic matter: (1) 1 g of soil was reacted with 150 mL NaOCl (15% active Cl) at 80 °C for 12 h, and (2) 1 g of soil was reacted with 100 mL of 0.1 *M* $Na_4P_2O_7$ at room temperature for 6 h. After each treatment step, soil suspensions were centrifuged for 1 h at 2800 g. The residue was washed with 40 mL of deionized water (milli-Q). The supernatant and washing solutions were stored at 5 °C in polyethylene bottles for ICP analyses; results are in Table 2.

Mine tailings (Leadville, Colorado, U.S.A.)

Leadville is located in central Colorado approximately 100 km southwest of Denver (Fig. 2). Mining and smelting in the Leadville area over the past 130 years generated large quantities of waste materials including waste rock, tailings, and slags. The potential health risks and environmental hazards posed by these wastes prompted the U.S. Environmental Protection Agency to place the Leadville, Colorado, area on its National Priority List (i.e., Superfund list) in 1983 under the Comprehensive Environmental Response Compensation and Liability Act (CERCLA). Two chemically distinct tailings piles in Leadville were sampled; the Hamms tailings contains abundant carbonate and has a near-neutral soil pH (6 to 8), whereas the Apache tailings is dominated by sulfides (especially pyrite) and has a correspondingly low soil pH (2 to 6) (ASARCO 1993). Additional analyses of these and other tailings materials from Leadville, including evaluation of changes in speciation with chemical extractions, are presented by Ostergren et al. (unpublished manuscript).

Fine fractions were isolated from the bulk by sedimentation according to Stokes Law. Chemical analyses of the <100 μm fractions were conducted by ICP with aqua regia digest by XRAL Laboratories (Ontario, Canada) (Table 1). EXAFS analyses were conducted on <10 μm and <5 μm fractions for the Hamms and Apache samples respectively.

TABLE 2. Percentages of metal removed by chemical extractions from the <2 μm topsoil fractions

	$CaCl_2$ (0.5 *M*)		NaOCl (80 °C)		$Na_4P_2O_7$ (0.1 *M*)	
	Tilled	Wooded	Tilled	Wooded	Tilled	Wooded
Pb	0.0	38.1	34.6	70.8	44.0	77.0
Zn	2.4	37.5	5.3	6.0	25.0	57.0
Fe	0.0	0.00	1.2	1.2	3.0	15.0
Mn	2.3	27.8	0.3	0.5	10.0	52.0
Al	0.0	0.0	1.8	1.2	3.2	0.2
Si	0.0	0.0	1.5	1.6	0.0	0.1

Reference samples for Pb^{2+} adsorbed species

In addition to crystalline model compounds, three synthetic sorption samples were used as reference compounds for EXAFS analysis of natural samples. The Pb^{2+}-humate sample was prepared at pH 6 by reacting a purified natural humic acid placed in a dialysis membrane with an external $Pb(NO_3)_2$ solution for 24 h (Boisset, 1995). Pb^{2+} adsorbed on synthetic birnessite (BET surface area ≈ 200 m^2/g) was prepared by base titration to pH 6 of a 10 g/L birnessite suspension in 0.1M $NaNO_3$ containing 7×10^{-4} *M* total Pb, added from an acidified 0.1 *M* stock solution of Pb nitrate. Pb^{2+} adsorbed to synthetic goethite (BET surface area 45 m^2/g) was prepared by base titration to pH 7 of a 0.5 g/L goethite suspension in 0.1 *M* $NaNO_3$ containing 5×10^{-5} *M* total Pb. The Pb^{2+} on goethite model was equilibrated with laboratory atmo-

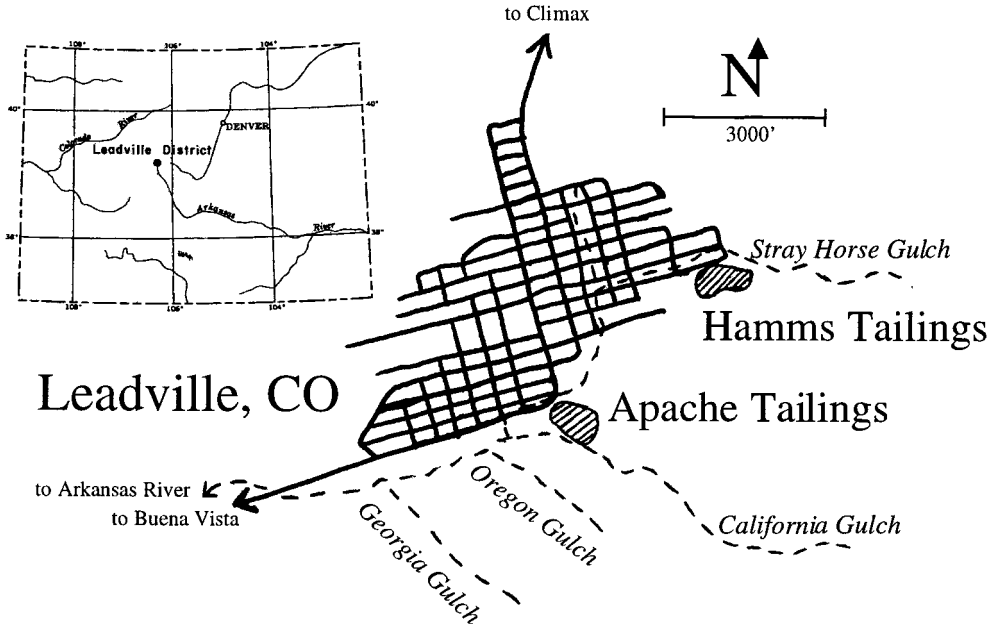

FIGURE 2. Leadville, Colorado, location map showing Hamms and Apache Tailings piles.

sphere, and the Pb^{2+} on birnessite model was prepared in the absence of CO_2 under a continuous flow of Ar. Final concentrations of dissolved Pb were subsaturated with respect to known solid phases (i.e., hydrocerussite and basic Pb nitrate). Lead concentrations in the sorption models were 1 wt% in the humate sample, 2 μmol/m² for Pb on goethite, and 0.4 μmol/m² for Pb on birnessite.

EXPERIMENTAL METHODS

The mineralogical compositions of the soil fractions (bulk samples, fine fractions, and dense fractions) were determined by powder XRD using Co*K*α radiation (40 kV, 30 mA) operating in step scan mode. XRD data were collected between 2θ of 3 and 100° with a 0.04° step and a counting time of 20 s per step on the Evin-Malmaison samples, and between 5–100° 2θ with a 0.03° 2θ step and counting time of 5 s per step on the Leadville samples. Microscopic observations were conducted with a scanning electron microscope (SEM) equipped with an energy dispersive spectrometer (EDS) for chemical analyses (JEOL JSM 840A in Paris, and JEOL Superprobe 733 at Stanford). Compositional analyses of individual points on soil and mine tailings particles, as well as elemental maps and transects, were performed by electron microprobe equipped with wavelength dispersive spectrometers (WDS) (SX50 CAMEBAX in Paris, and JEOL Superprobe 733 at Stanford). For these microscopic observations and analyses, samples were embedded in epoxy resin and prepared as thin sections mounted on pure silica SUPRASIL slides. Additional microscopic observations and analyses were conducted on particles separated from the bulk on the basis of density and/or magnetism after mounting these particles on Scotch tape.

Synchrotron-based X-ray micro-fluorescence (μSXRF)

The distribution of Pb in each Evin-Malmaison sample was assessed by micro-SXRF on thin sections. Data were collected at room temperature on bending magnet beam line D15A at the Laboratoire pour l'Utilisation du Rayonnement Electromagnetique (LURE, Orsay, France). This beam line is equipped with a Bragg-Fresnel lens that yields a monochromatic 13.6 keV beam focused to a 25 μm diameter spot. Micro-SXRF mapping was performed in step scanning mode on 1 mm² areas, with 20 μm steps and a counting time of 20 s per step. Metal concentrations are represented in terms of number of counts because of the difficulty of applying reliable absorption corrections as a function of the local chemical composition at each analysis point.

Extended X-ray absorption fine structure spectroscopy (EXAFS)

EXAFS data for all samples were recorded on wiggler beamline IV-3 at the Stanford Synchrotron Radiation Laboratory (SSRL, Stanford, California, U.S.A.) using Si(220) or Si(111) monochromator crystals. Energy was calibrated using a Pb-metal foil; the first inflection of the Pb metal L_{III} absorption edge was set to 13038 for the French samples and 13055 for the Leadville samples, and E_0 for EXAFS was defined as 13055 (17 eV above Pb metal first inflection) and 13070 (15 eV above Pb metal first inflection) for French and Leadville samples respectively. These differences in data treatment resulted in a systematic shift in EXAFS *k* values between the two data sets and explain apparent discrepancies between the model spectra used for each set of samples. Pb L_{III}-edge data were collected in fluorescence mode using a high

throughput (120 kcts/s) Canberra 13-element Ge detector. A Se (6T) filter was used to attenuate elastic scattering, and Cr, V, and/or Al filters were used to attenuate Fe fluorescence from sample matrices. Data from the Leadville mine tailings samples were recorded at room temperature, and the Evin-Malmaison soil samples were recorded at 10 to 20 K.

EXAFS data were fit using both conventional non-linear least-squares fitting of individual coordination shells (hereafter referred to as shell fitting) and direct fitting of $k^3\chi(k)$ functions by least-squares optimization of linear combinations of empirical model spectra (hereafter referred to as empirical fitting). Theoretical phase-shift and amplitude functions employed for shell fitting were generated using FEFF 6 (Zabinsky et al. 1995). This fitting was done using EXAFSPAK (George and Pickering 1993) for the Leadville samples and FITEX (Bonnin et al. 1985) for the Evin-Malmaison samples. Fitting of Pb-O shells was performed using FEFF-generated phase shift and amplitude functions for α-PbO. Fitting of EXAFS data from well-characterized model compounds including α-PbO and cerussite ($PbCO_3$) using these functions provided an estimate of the accuracy of Pb-O distances (±0.02 Å) and number of neighbors (±20% for undistorted first-shell). Phase-shift and amplitude functions for Pb-Fe and Pb-Mn shells were calculated using FEFF6 from the structures of magnetoplumbite ($PbFe_{12}O_{19}$; Moore et al. 1989) and coronadite ($PbMn_8O_{16}$; Post and Bish 1989) respectively. This protocol helped assess the accuracy of our EXAFS-derived Pb-Fe and Pb-Mn bond distances and coordination numbers, which were ±0.04 Å and ±20% respectively (cf. O'Day et al. 1994). One other important use of FEFF is to check for multiple-scattering effects, which can be an important contributor to second-shell amplitudes in EXAFS spectra.

Because conventional shell-by-shell EXAFS fitting in complex multi-component systems can quickly lead to impractically large numbers of fitting parameters, especially for Pb species whose coordination environments are both complex and highly variable, most of the samples were analyzed using direct least-squares fitting of the $k^3\chi(k)$ functions. Because EXAFS spectra are normalized to a per-atom basis, the fraction of total Pb residing in a particular component (mineral phase or other coordinatively distinct species) is expressed directly by the fraction of the corresponding model spectrum contributing to the fit. Identifying species by this method relies upon EXAFS spectra and combinations of spectra being unique and distinctive. Although a diversity of local coordinations generally make Pb L_{III}-EXAFS distinct from each other, these fits must be guided and constrained as much as possible by complementary techniques, such as EPMA, to avoid missing or misidentifying components. Application of this linear least-squares fitting procedure to known mixtures of Pb model compounds provides results that are generally accurate to within ±25% of the actual atomic fractions present and is capable of identifying contributions on the order of 10% (Ostergren et al., unpublished manuscript, for further discussion).

Twenty-three Pb L_{III} reference $k^3\chi(k)$ functions from different compounds were compiled and used for this fitting (Ostergren et al., unpublished manuscript). Crystalline models were chosen to represent phases identified by EPMA in the Leadville tailings (Pb oxides, sulfates, phosphates, chlorides, sulfide, and vanadate). The model set used here also included synthetic samples of Pb^{2+} adsorbed to Fe hydroxide, Mn oxide, and humic acid, which were recognized as potentially relevant substrates for Pb adsorption in both the Leadville and Evin-Malmaison samples as suggested by μSXRF, EPMA, and chemical extractions.

Model compounds for adsorbed Pb^{2+} species

Pb^{2+}-humate. EXAFS data of a Pb-humate prepared at pH 6 and containing 1% Pb by weight are presented in Figure 3e. The Pb-O distance obtained from fitting of the first radial distribution function (RDF) peak (2.41 ± 0.02 Å) agrees with that reported by Xia et al. (1997) from a room temperature EXAFS analysis of synthetic Pb-humate prepared at pH 5 (Pb-O = 2.40 Å). These investigators also reported a Pb-C contribution ~3.25 Å, suggesting that Pb is sorbed as inner-sphere complexes on humic substances. In the present study where EXAFS measurements were carried out at 10 K and the *k*-range is larger than in the work of Xia et al. (up to 10 $Å^{-1}$ instead of 8 $Å^{-1}$), the small second-neighbor contribution ($R + \Delta = 2.8$ Å) observed in the RDF of the Pb-humate spectrum (Fig. 3e) could not be fit with only one C shell. Because of the small amplitude of this contribution with respect to the Fourier ripple of the first-shell peak ($R + \Delta = 1.2$ Å), no further analysis of this contribution was attempted for the synthetic or natural samples. Therefore, no conclusion can be drawn from these EXAFS data regarding the inner- or outer-sphere character of the Pb-humate complexes, although macroscopic adsorption isotherm studies suggest that Pb is bound mainly to humic substances as inner-sphere complexes (Kinniburgh et al. 1996).

Pb^{2+} adsorbed on goethite. The Pb L_{III}-EXAFS spectrum of Pb sorbed on goethite is dominated by a first-neighbor contribution at $R + \Delta = 1.9$ Å with a small second-neighbor contribution at $R + \Delta = 3.1$ Å (Fig. 3d). Fitting these features gave Pb-O and Pb-Fe distances (2.28 ± 0.02 and 3.35 ± 0.04 Å respectively) that closely agree with those reported previously for Pb on goethite and hematite (Bargar et al. 1997b) and on hydrous ferric oxide (Manceau et al. 1992) (Table 3). These distances indicate bidentate Pb adsorption complexes that share edges with $Fe(O,OH)_6$ octahedra.

Pb^{2+} adsorbed on birnessite. EXAFS data for a synthetic sample of Pb sorbed on birnessite are presented in Figure 3g. The Pb-O distance of 2.31 ± 0.02 Å derived from fitting of the first RDF peak is similar to that reported by Manceau et al. (1992) and Boisset (1995). The RDF shows a strong peak at R + Δ = 3.4 Å, and

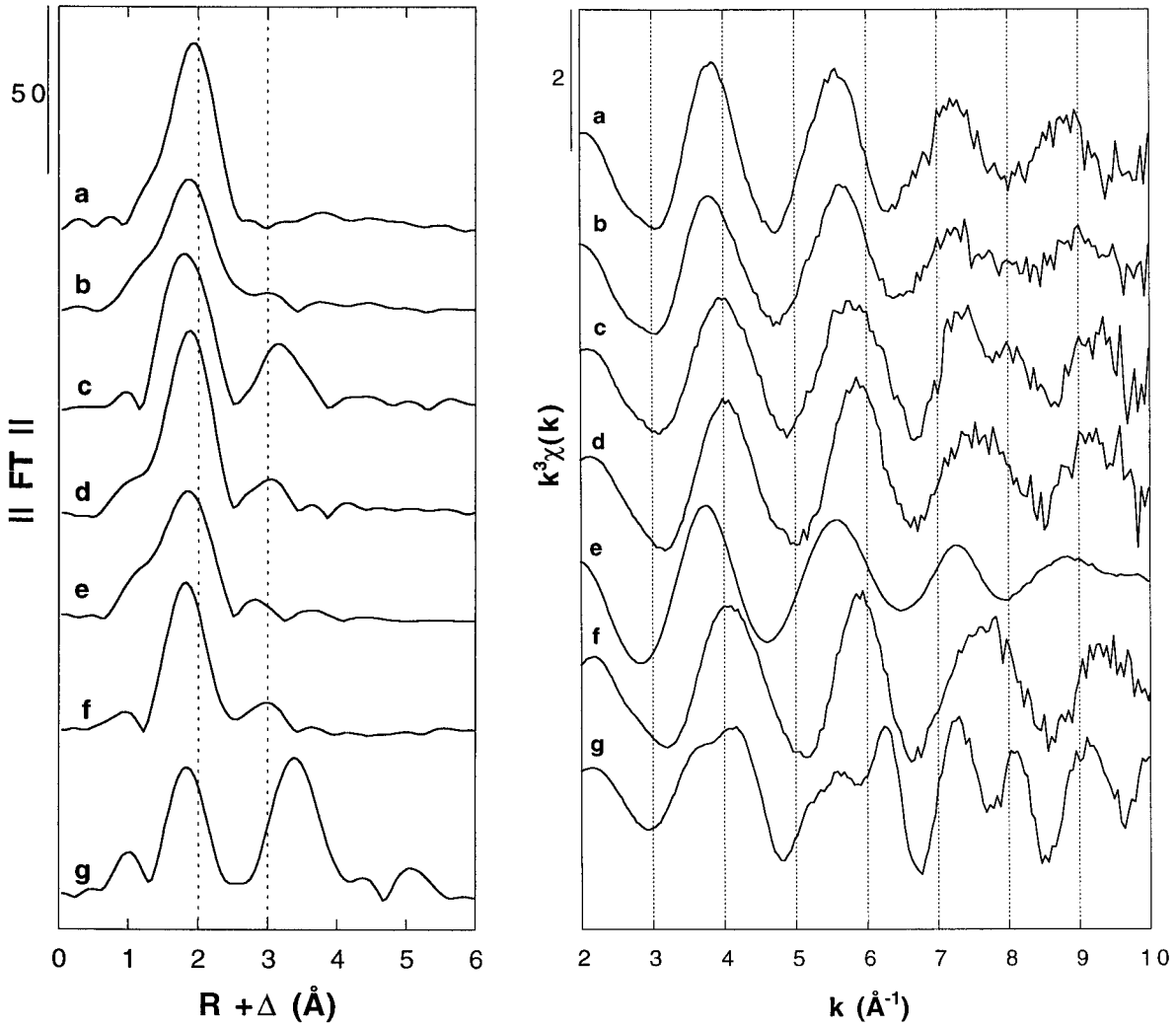

FIGURE 3. Pb L_{III}-EXAFS $k^3\chi(k)$ functions (right) and RDFs (left) of (**a**) wooded topsoil fine fraction, (**b**) $CaCl_2$ treated wooded topsoil fine fraction, (**c**) tilled topsoil fine fraction, (**d**) $Na_4P_2O_7$ treated tilled topsoil fine fraction, (**e**) synthetic Pb^{2+} humate, (**f**) Pb^{2+} adsorbed on synthetic goethite, and (**g**) Pb^{2+} adsorbed on synthetic birnessite.

the fitting of only one Pb-Mn distance (3.74 ± 0.02 Å) was necessary to account for this second-neighbor contribution (Table 3). These distances are interpreted as corner-sharing Pb complexes located above and below vacancies in the MnO_2 layers of the birnessite structure. This model is in agreement with that reported by Boisset (1995) and is similar to the model proposed for Zn sorbed on birnessite by Manceau et al. (1992) where Zn^{2+} ions were found to have the same short-range environment as in the chalcophanite structure. The Pb-Pb correlations reported by Manceau et al. (1992) for Pb on birnessite, which were not observed in the present Pb on birnessite sorption sample, could be due to the higher Pb concentration in their sample (5 wt%) relative to this study (1.6 wt%) or the study of Boisset (1995) (0.2 and 0.9 wt%).

RESULTS AND DISCUSSION

Smelter impacted soils (Nord-Pas-de-Calais, France)

Bulk Pb concentrations in both soils (Fig. 4) are well above natural background levels and highest at ground surface. In the tilled soil, Pb concentrations are relatively constant (averaging 460 ppm) in the upper 30 cm, reflecting the physical homoginization of tillage. Just below this tilled horizon, the Pb concentration falls to about 20 ppm, which is typical of the average background level of Pb in soils (Krauskopf 1992). In the wooded soil, which has not been disturbed by human activity for the past 50 years, the Pb concentration decreases continuously from the ground surface (maximum 1900 ppm in the topsoil), reaching background levels (15 to 20 ppm) at 50 cm depth. These trends with depth, combined with the aerial

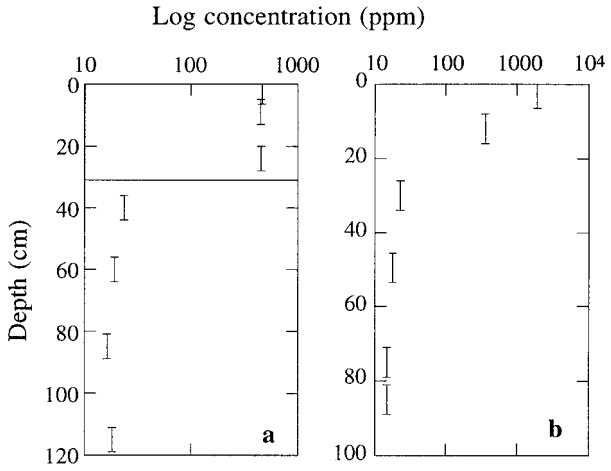

FIGURE 4. Profiles of Pb concentrations as a function of depth in (**a**) tilled soil and (**b**) wooded soil of Evin-Malmaison. The grey area for the tilled soil profile corresponds to the tilled horizon (0–30 cm).

distribution of Pb about the smelter (Fig. 1), suggests that anomalous Pb in these soils is related to smelter emissions.

The spatial distribution of Pb on the 20 μm scale was investigated using μSXRF. Two major Pb associations can be distinguished in a elemental map obtained for Pb, Fe, and Mn on the surface horizon of the wooded soil (Fig. 5). Pb is concentrated in Fe- and/or Mn-rich dark silty and sandy heterogeneous aggregates. In addition, Pb is always detected in finely divided clayey matrices with embedded quartz grains. A strong correlation is observed between Pb and Mn, especially for high Pb and Mn levels, whereas the correlation was poorer for Pb and Fe. This latter correlation, however, is better for low Pb levels (i.e., in the finely divided soil matrix). This spatial distribution of metals, as well as these chemical correlations were systematically observed in the μSXRF maps collected from the top-soil horizons of both tilled and wooded soils.

Dense fractions. Quantitative analysis by Rietveld refinement of XRD data from dense particles separated from the 2 to 200 μm fraction extracted from the wooded topsoil showed a mixture of high-temperature phases with 46 wt% hematite, 30 wt% magnetite, and 2 wt% wüstite associated with minor amounts of minerals inherited from the bedrock (11 wt% quartz, 6 wt% rutile, and 3.5 wt% anatase). The presence of magnetite in high concentrations explains why most of these dense particles were magnetic. No Pb-bearing minerals were identified by XRD in these materials. As revealed by SEM-EDS, Pb is primarily present in glass-like particles with filamentary shapes and displays an association with Si-Fe-Ca-Al-Pb-Zn and with minor P (Fig. 6). This association was confirmed by EPMA, and the Pb concentration ranges from 0.5 to 9 wt%. EXAFS spectra of the dense fractions (data not shown) strongly differ from those of the fine fractions (discussed in the next section). Interpretation of EXAFS data from the dense fractions is still underway, and no match was found with the model compounds available for this study, including alamosite ($PbSiO_3$), plumboferrite ($PbFe_4O_7$), and magnetoplumbite ($PbFe_{12}O_{19}$). The combination of XRD, SEM, and EPMA data suggest that Pb in the dense fractions of both soils was partly incorporated in the glassy matrix of Si-Fe-Ca-Al-Pb-Zn grains. The morphology and chemical composition of these grains, in addition to the mineralogy of crystalline materials in the dense fraction, indicate that these are slag materials created by a high-temperature smelting process. Furthermore, these Pb-bearing glassy particles are small enough to have been transported by wind from the factory wastes. Cracks that may have formed during rapid cooling, which were enlarged and smoothed by dissolution processes as observed in SEM photographs (Fig. 6), support the hypothesis that Pb in these particles may be redistributed with time. These slag materials could then represent significant sources for Pb contamination in the soils studied, although smelter aerosols containing lead sulfide and sulfate (Clevenger et al. 1991) may also have contributed significantly to the contamination.

Other Pb-rich grains whose chemical compositions differ significantly from those of the slag grains were also recognized in the dense fraction of the 2 to 200 μm material. These grains exhibit compositions typical of hydrous iron oxides and/or hydrous manganese oxides and contain up to a few weight percents in Pb. Elemental maps with micrometer-scale resolution obtained using EPMA on the topsoil thin sections indicate the presence of several of these types of grains in both topsoils (Fig. 7). The absence of Al and Si and the high amounts of Fe and Mn indicate that these aggregates consist of hydrated iron and manganese oxides embedded in a matrix of quartz grains. The frequent association of Pb with such soil aggregates strongly suggests that hydrated iron and manganese oxides play a significant role as a sink for heavy metals in the soils studied. A preferential association of Pb with the Mn-rich aggregates or with the Mn-rich core of mixed aggregates of Fe- and Mn-oxides was observed on several elemental maps (Fig. 7). This observation is in agreement with the high affinity of Pb for manganese oxide surfaces (Alloway 1995, and references therein).

The association of Pb with Fe and Mn oxide aggregates, as well as the systematic presence of Pb in the finely divided soil matrix, can be interpreted as evidence of Pb remobilization in the soils studied. Aerially deposited lead, as well as lead released by the dark silty grains, reacts with the finely divided matrix comprised of clays, organic matter, and Fe-, Al-, and Mn-oxyhydroxides.

Fine fractions (<2 μm). Compositional analyses indicate that the isolated fine fraction (<2 μm) is enriched twofold and fourfold in Pb with respect to the bulk samples of the wooded and tilled topsoils (Table 1). Moreover, the fine fraction accounts for 16 wt% and 20 wt% of the tilled and wooded topsoil layers, respectively, and

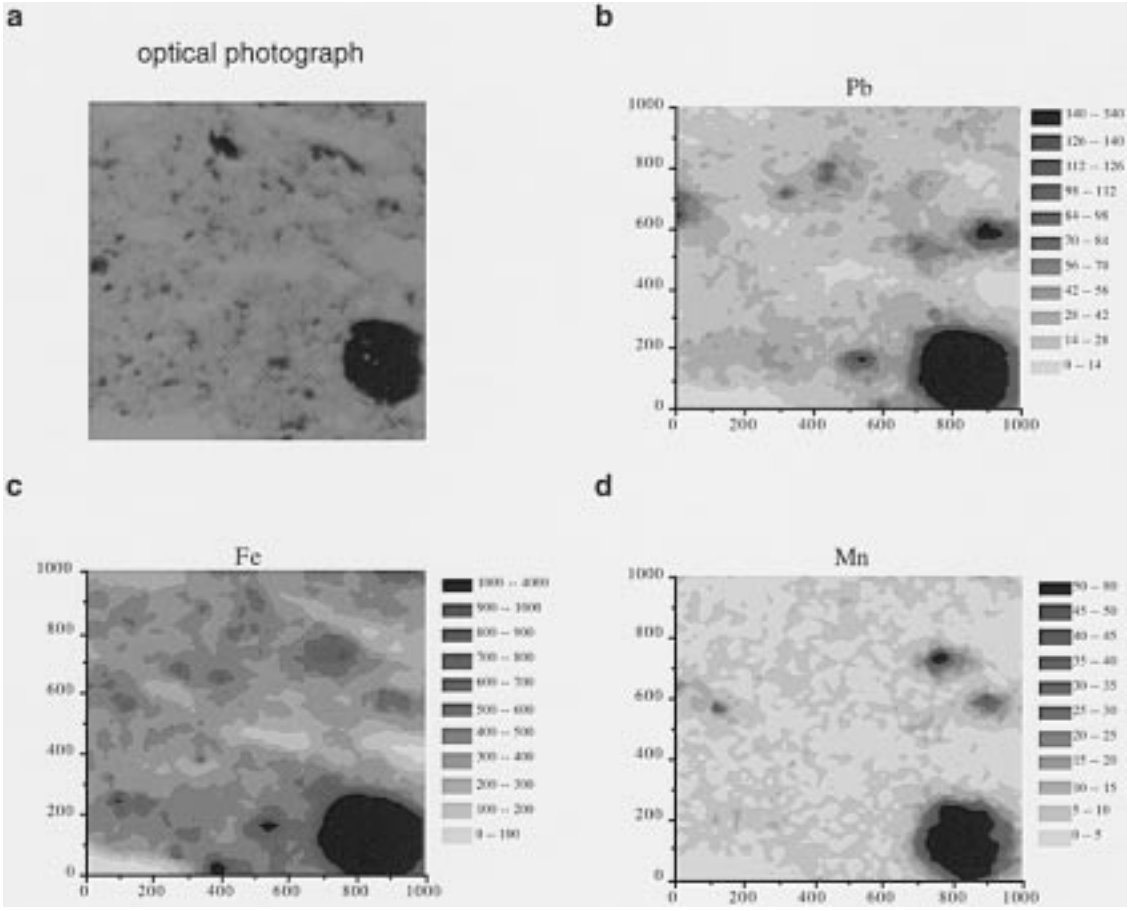

FIGURE 5. Optical photograph (**a**) of a 1 × 1 mm area on a thin section of the tilled topsoil and corresponding elemental maps obtained by μSXRF for Pb (**b**), Fe (**c**), and Mn (**d**). μSXRF concentration unity is arbitrary (counts).

therefore represents about 70 wt% and 45 wt% of the total Pb in the tilled and the wooded topsoils respectively. XRD powder spectra of the fine fractions of both topsoils indicate that they contain primary minerals inherited from the bedrock (consisting mainly of quartz and orthoclase), as well as clay minerals (smectite, illite, and kaolinite). No Pb-bearing minerals were identified by XRD in the fine fractions of both topsoils. In addition, EPMA and SEM-EDS analyses provided no evidence of any chemical correlations between Pb and other elements in these clayey materials, although μSXRF analyses suggest that Pb is present in association with Fe and Mn in these fractions. EXAFS spectroscopy combined with chemical extractions was used to probe the molecular environment of Pb in this soil compartment.

Figure 3 displays the Pb L_{III}-edge EXAFS spectra and the RDFs of the fine fraction from both topsoils, before and after chemical extractions, and of reference compounds for sorbed Pb species. Before chemical extractions, the RDF of the tilled topsoil (Fig. 3c) exhibits a second-neighbor contribution at $R + \Delta = 3.1$ Å, whereas no second-neighbor contribution is present in the RDF of the wooded topsoil (Fig. 3a). The second-neighbor contribution in the EXAFS data from the tilled topsoil is readily observed in the $k\,^3\chi(k)$ function (Fig. 3c) where an additional oscillation around $k = 8$ Å^{-1} is superimposed on the first-neighbor oscillation. In contrast, only one frequency is observed in the $k\,^3\chi(k)$ function of the wooded topsoil (Fig. 3a). These data show that Pb speciation differs between the tilled and wooded topsoils. The presence of a second-neighbor peak in the tilled topsoil RDF suggests that Pb occurs mainly as inner-sphere complexes at the surface of mineral components or is incorporated in mineral structures in this soil. In contrast, the absence of a second-neighbor peak in the wooded soil RDF may indicate that a significant amount of Pb occurs as outer-sphere complexes or as inner-sphere complexes sorbed on a light matrix (e.g., humic substances) that cannot be detected using Pb-EXAFS spectroscopy. Differences in the chemical form of Pb between the two topsoils is also indicated by the smaller first-neighbor distance in the tilled topsoil ($R + \Delta = 1.8$ Å), whereas it is slightly shifted to a longer distance ($R + \Delta = 1.9$ Å) in the wooded topsoil. This difference is illustrated in the phase-shift observed between both $k\,^3\chi(k)$ functions.

Quantitative analysis of EXAFS data, before and after

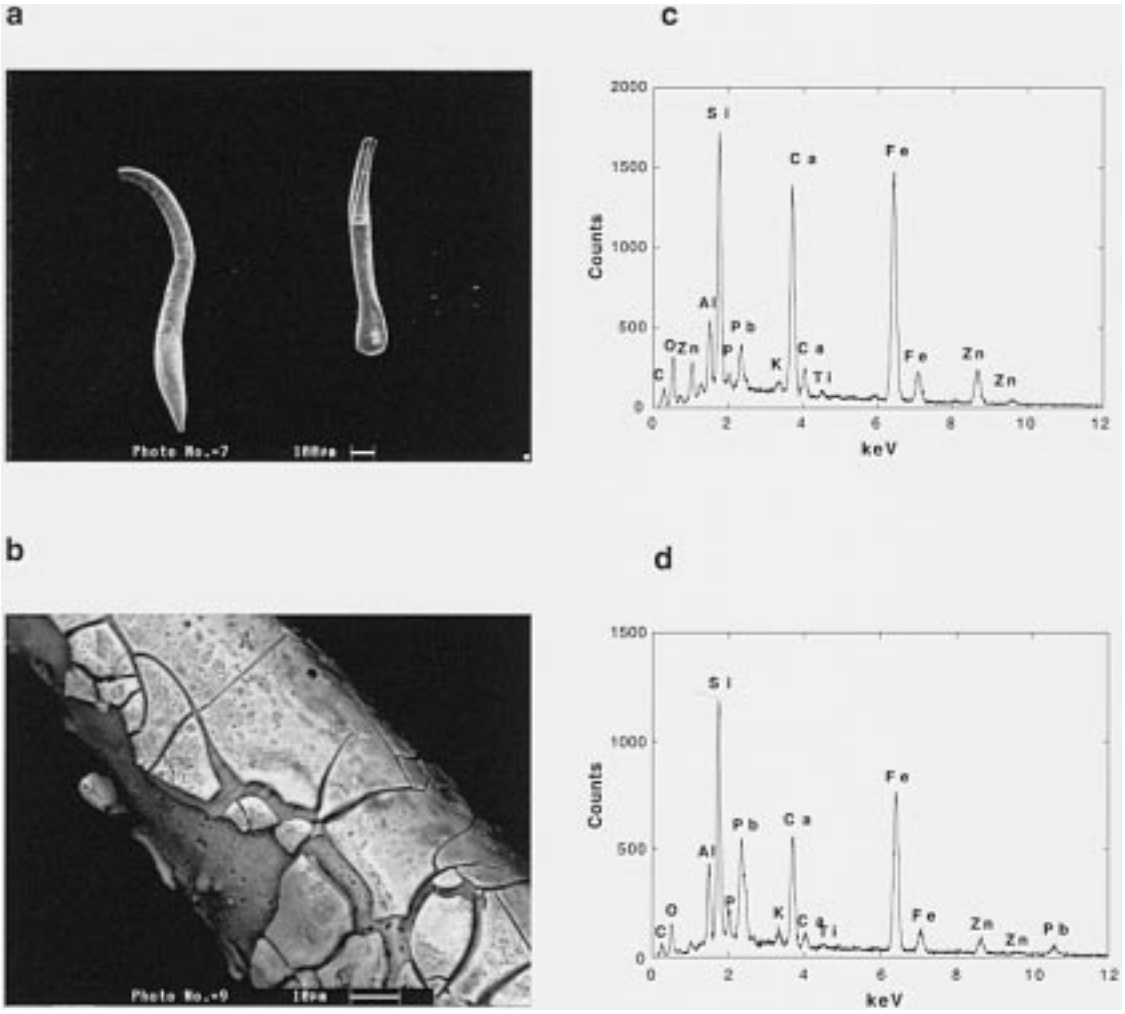

FIGURE 6. SEM photographs (**a** and **b**) and EDS analyses (**c** and **d**) of dense materials extracted from the wooded topsoil. Note the filament shape of these glass-like particles (**a**) and micro-fractures on their surfaces produced during cooling (**b**).

chemical treatment of the samples using quantitative comparison with reference compounds by least-squares fitting and conventional shell-by-shell fitting, was performed to fully determine Pb speciation in the fine fractions of both topsoils.

Fine fraction (<2 μm) of the wooded topsoil. The qualitative match between the $k^3\chi(k)$ function of the untreated and $CaCl_2$-treated samples (Fig. 3a and 3b) and that of synthetic Pb-humate (Fig. 3e) suggests that a large portion of the Pb is bound to organic matter in the fine fraction of the wooded topsoil. The occurrence of organo-lead species as the main form of Pb in the wooded topsoil is strongly indicated by least-squares fitting of the $k^3\chi(k)$ function of the $CaCl_2$-treated sample. In addition, the occurrence of a small amount of Pb sorbed on ferric hydroxides is also suggested by linear least-squares fitting of the EXAFS data, which gives a mixture of 80% Pb-humate and 20% Pb sorbed on goethite (Fig. 8a). The same least-squares procedure was applied to the EXAFS data from the untreated fine fraction, but it yielded poorer agreement in the amplitudes of the first-neighbor oscillations.

Shell fitting of the EXAFS data was carried out to better constrain Pb speciation. The wooded topsoil fine fractions before and after $CaCl_2$ treatment, which extracted 38% of the Pb (Table 2), have similar $k^3\chi(k)$ functions (Fig. 3a and 3b). However, in the $CaCl_2$-treated sample, the position of the maximum of the first peak of the RDF shifts toward smaller distances, and its apparent amplitude decreases. Fits of the first-shell contributions in the $CaCl_2$-treated sample indicated a slight shortening of the Pb-O distance (Pb-O = 2.39 ± 0.02 Å) relative to the untreated sample (Pb-O = 2.42 ± 0.02 Å). Despite this difference, the first-neighbor contributions obtained for the untreated and the $CaCl_2$-treated samples are both similar to that in synthetic Pb-humate (Pb-O = 2.41 ± 0.02 Å). The presence of organo-lead complexes in the wooded topsoil is also supported by the large amounts (70.8 and 77.0%) of Pb released from the raw fine fraction by NaOCl and $Na_4P_2O_7$ treatments, respectively (Table 2).

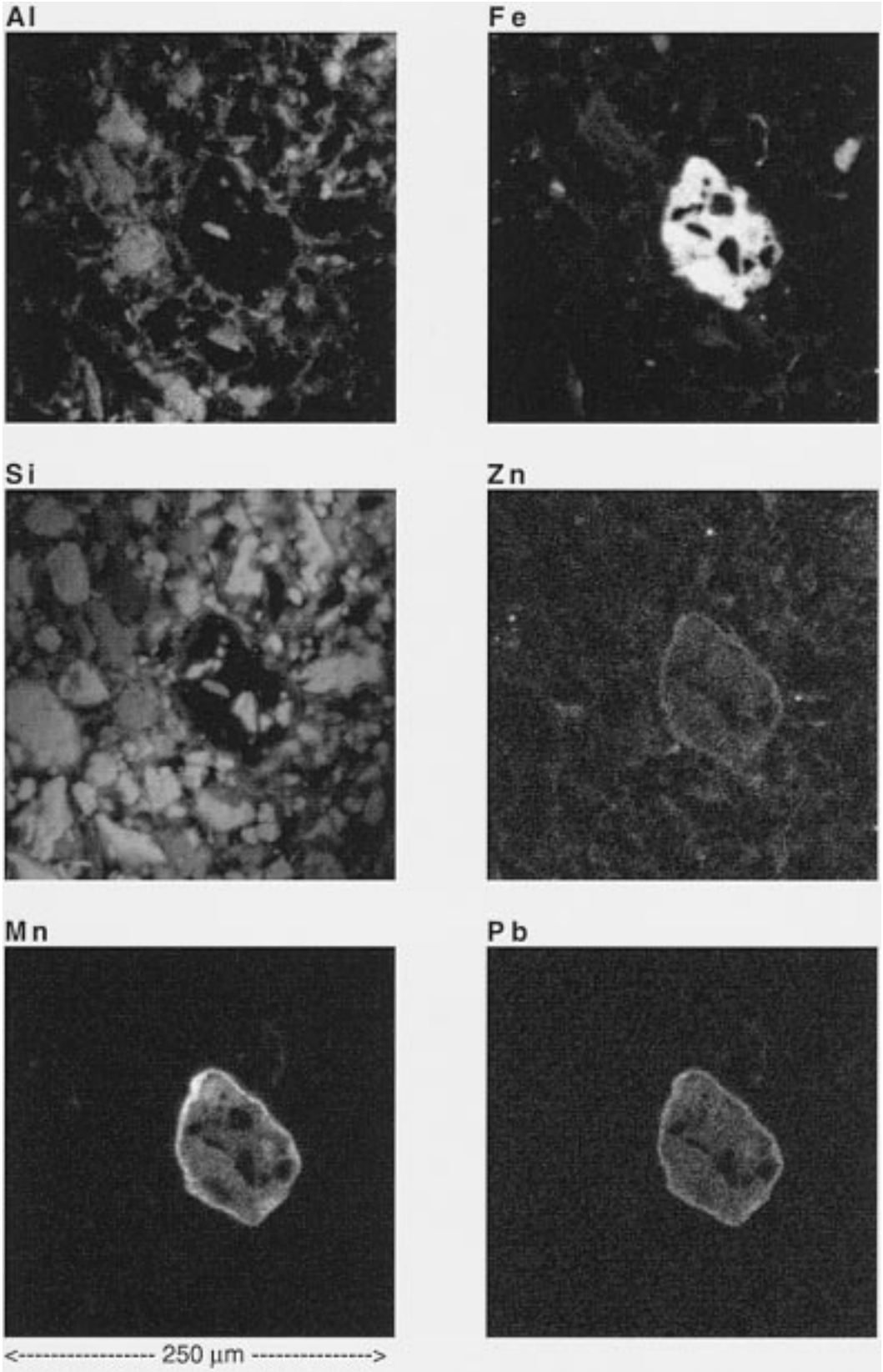

FIGURE 7. EPMA elemental maps (Al, Fe, Si, Zn, Mn, and Pb) from a thin section of the tilled topsoil showing Pb and Zn association with a Fe, Mn oxide.

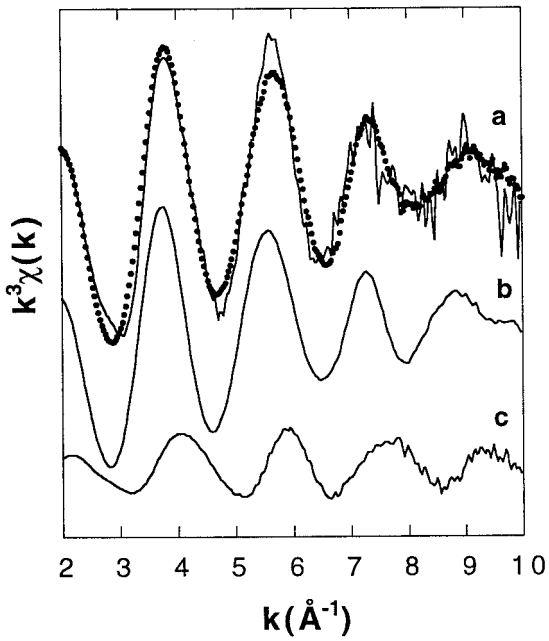

FIGURE 8. Linear least-squares fitting of the Pb L_{III}-EXAFS $k^3\chi(k)$ functions from the $CaCl_2$ treated wooded topsoil fine fraction. (**a**) Experimental (plain line) and calculated (dotted line), (**b**) 80% synthetic Pb^{2+} humate, and (**c**) 20% Pb^{2+} adsorbed on synthetic goethite.

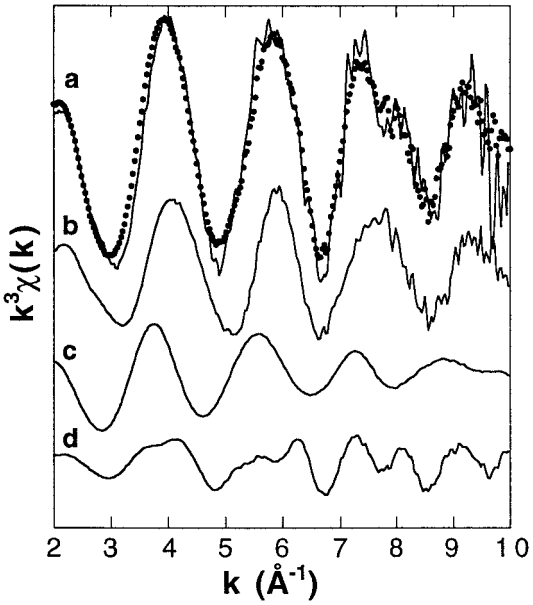

FIGURE 9. Linear least-squares fitting of the Pb L_{III}-EXAFS $k^3\chi(k)$ functions from the tilled topsoil fine fraction. (**a**) Experimental (plain line) and calculated (dotted line), (**b**) 45% Pb^{2+} adsorbed on synthetic goethite, (**c**) 35% synthetic Pb^{2+} humate, and (**d**) 20% Pb^{2+} adsorbed on synthetic birnessite.

However, these treatments overestimate the fraction of organo-lead species, because the sums of the $CaCl_2$-extractable Pb (38.1%) and the NaOCl extractable Pb (70.8%) or $Na_4P_2O_7$ extractable Pb (77.0%) are larger than 100%. In addition, the slightly shorter average Pb-O distance (2.39 ± 0.02 Å) in the $CaCl_2$-treated sample is consistent with an additional contribution from Pb complexes sorbed on ferric hydroxides with shorter Pb-O distances (2.30 ± 0.02 Å, Table 3). Furthermore, the RDF of the $CaCl_2$-treated sample shows a small second-neighbor contribution at R + Δ = 3.0 Å which is also present in the RDF of Pb sorbed on goethite, although this contribution in the $CaCl_2$-treated sample was too weak to yield definitive fitting results.

The larger Pb-O distance in the untreated sample (2.42 ± 0.02 Å) than in the $CaCl_2$-treated sample (2.39 ± 0.02 Å) can be explained by the occurrence of a significant amount of exchangeable outer-sphere Pb species (38.1% as indicated by $CaCl_2$ extraction) in association with organo-lead species and Pb sorbed on ferric hydroxides, as previously recognized in the $CaCl_2$-treated sample. Indeed, Pb-O distances for outer-sphere Pb species should be close to that for aqueous Pb^{2+} (Pb-O = 2.45 Å; Bargar et al. 1996; Farquhar et al. 1997). The presence of outer-sphere Pb species could explain the relatively poor fit of the $k\ ^3\chi(k)$ function of the untreated sample obtained using a linear combination of only Pb-humate and Pb sorbed on goethite, although it is also possible that another sorbed-Pb model compound could improve the fit.

Fine fraction (<2 μm) of the tilled topsoil. The occurrence of a second-neighbor contribution in the RDF of the tilled topsoil fine fraction (Fig. 3c) indicates that Pb is either incorporated in mineral phases or is sorbed as inner-sphere complexes on mineral surfaces. Both hypotheses are in agreement with the absence of $CaCl_2$-extractable Pb (Table 2), which suggests that no Pb is present as outer-sphere complexes in this sample.

The best fit of the $k\ ^3\chi(k)$ function for this sample was obtained with a mixture of 45% Pb sorbed on goethite, 35% Pb-humate, and 20% Pb sorbed on birnessite (Fig. 9). No match was found with crystalline phosphates (e.g., pyromorphite) or carbonates (e.g., cerussite or hydrocerussite). This result is supported by qualitative analysis of the RDF functions; the second-neighbor contribution at $R + \Delta = 3.3$ Å observed in the RDF's of the tilled topsoil fine fraction can be interpreted as a mixture of the weak second-neighbor RDF contribution at $R + \Delta = 3.0$ Å observed for the Pb sorbed on goethite sample and the sharp second-neighbor RDF contribution at $R + \Delta = 3.4$ Å observed for the Pb sorbed on birnessite sample. This interpretation is confirmed by the fitting of the second shell of the tilled topsoil RDF, which yields 0.2 Fe/Mn at 3.36 ± 0.02 Å and 0.3 Fe/Mn at 3.70 ± 0.02 Å (Table 3). The short distance is similar to that of the Pb-Fe contribution for Pb^{2+} sorbed on goethite (3.35 ± 0.02 Å) and indicates that a fraction of Pb^{2+} was sorbed on Fe hydroxides [bidentate Pb^{2+} adsorbed to edges of $Fe(O,OH)_6$ octahedra]. The long distance is slightly shorter than that for Pb^{2+} sorbed on birnessite (3.74 ± 0.04 Å), which may reflect some influence of the shorter Pb-Fe distance. The

TABLE 3. Results of EXAFS data analysis for natural samples and synthetic model compounds

Sample	First-shell (Pb-O)			Second-shell (Pb-Ct)			ΔE_0
	R (Å)	N	σ (Å)	R (Å)	N	σ (Å)	(eV)
Leadville Tailings							
Hamms <10 μm	2.29	1.6	0.1	3.32	0.3	0.1	−7.7
Apache <5 μm	n.i.	n.i.	n.i.	3.55	5.9	0.13	0
Evin-Malmaison soils							
Wooded soil <2 μm	2.42	2.4	0.09	n.o.	n.o.	n.o.	2.3
Wooded soil <2 μm $CaCl_2$ treated	2.39	2.5	0.12	n.i.	n.i.	n.i.	0.9
Tilled soil <2 μm	2.34	2.2	0.11	3.36	0.2	0.06	0.8
				3.70	0.3	0.06	
Tilled soil <2 μm NapP treated	2.33	2.2	0.10	3.39	0.4	0.08	−0.9
				3.57	0.2	0.08	
Pb^{2+} adsorbed on humic acid	2.41	2.8	0.12	n.i.	n.i.	n.i.	2.4
Pb^{2+} adsorbed on birnessite	2.31	1.3	0.09	3.74	2.0	0.09	1.4
Pb^{2+} adsorbed on goethite	2.28	2.6	0.1	3.35	0.6	0.1	−7.7

Notes: N = EXAFS derived coordination number (±20% for undistorted first-shell neighbors), R = interatomic distance (±0.02 Å for the average Pb-O bonds and ±0.04 Å for Pb-Ct bonds), σ (Å) = Debye Waller factor. ΔE_0 (eV) values are referenced to α-PbO for all samples except the Apache Tailings, which is referenced to plumbojarosite. Pb-Ct corresponds to Pb-Fe for the ''Pb sorbed on goethite'' sample, to Pb-Mn for the ''Pb sorbed on birnessite'' sample and to Pb-Fe/Mn for the natural ''Tilled soil'' samples. n.i.: not interpreted; n.o.: not observed.

longer Pb-O distance derived for the tilled topsoil fine fraction (2.34 ± 0.02 Å) relative to the adsorption samples (2.28 ± 0.02 Å for Pb^{2+} adsorbed on goethite and 2.31 ± 0.02 Å for Pb^{2+} adsorbed on birnessite) can be explained by a significant proportion of Pb^{2+} being bound to organic matter (Pb-O = 2.41 ± 0.02 Å), as indicated by least-squares fitting of the $k\,^3\chi(k)$ function (Fig. 9). The presence of organo-lead species in this soil is further supported by the extraction of 34.6% and 44% Pb with NaOCl and $Na_4P_2O_7$ extractions respectively (Table 2). In addition, EXAFS analysis of the $Na_4P_2O_7$-treated sample indicates that this treatment also affected Pb species sorbed on Mn oxides, as indicated by the decrease in intensity of the RDF peak at $R + \Delta = 3.3$ Å and the absence of the shoulder at 8.0 $Å^{-1}$ in the $k\,^3\chi(k)$ function (Fig. 9). Miller et al. (1986) have reported that this treatment is able to remove metal species associated with manganese oxides. The qualitative matching of the $k\,^3\chi(k)$ function of the $Na_4P_2O_7$-treated sample with that of Pb^{2+} adsorbed on goethite suggests that this is the main form of Pb in this sample. EXAFS-derived distances for the tilled soil after $Na_4P_2O_7$ treatment (Pb-O = 2.33 ± 0.02 Å; Pb-Fe/Mn = 3.39 ± 0.02 Å) are fully consistent with this hypothesis (Table 3).

To summarize, EXAFS spectroscopy combined with chemical extractions and microanalyses indicate that Pb speciation is complex and highly variable in individual samples and among the wooded and tilled French soil samples. A portion of the Pb is present in slag materials generated by smelting activities at the Evin-Malmaison site. In addition, this study also demonstrates that Pb reacted with soil components, probably through the weathering of slag materials. In the fine fraction of the topsoil, the chemical forms of Pb differ between the tilled and untilled soils, although the origin of the contamination is similar. (1) In the wooded soil, a significant portion of Pb is present as outer-sphere complexes (≈40%) which is $CaCl_2$-exchangeable. The remaining Pb is mainly bound to organic matter, present as humic acids, probably as Pb^{2+} inner-sphere complexes (≈50%). A minor amount (≈10%) of Pb is present as Pb^{2+} adsorbed on hydrous Fe-oxides or Fe-oxyhydroxides. (2) In the tilled topsoil, Pb is mainly present as inner-sphere complexes adsorbed on hydrous Fe-oxides. The amount of Pb present as inner-sphere complexes adsorbed on hydrous Mn-oxides is relatively small in the fine fractions (≈20%). This could be due to the coarser size of the hydrous Mn oxide aggregates (2 to 50 μm) as suggested by EPMA and μSXRF mapping.

The higher amount of organo-Pb^{2+} complexes and the presence of a large amount of exchangeable outer-sphere Pb^{2+} in the wooded topsoil relative to the tilled topsoil may be both related to the higher organic matter content of the wooded topsoil (6.4 wt% TOC) vs. the tilled topsoil (1.5 wt% TOC) rather than to the slight difference in pH (5.5 for the wooded topsoil and 7.5 for the tilled topsoil). Moreover, it can be inferred that mineral surfaces may be coated by organic substances that may inhibit metal adsorption on these surfaces.

Mine tailings (Leadville, Colorado, U.S.A.)

No Pb-containing phases were detectable by XRD in the bulk or fine fractions of either of the Leadville tailings piles, whereas several Pb-bearing phases were readily detected by EPMA. Both tailings contain galena (PbS), Pb-phosphates, Pb-vanadates, and Pb associated with Fe and/or Mn-rich hydrous oxides. Each of these phases was identified in both the bulk and fine (<100 μm) fractions, but the abundance of galena was dramatically reduced in the fine fractions. Pb-bearing Fe-rich (hydroxy)sulfates and Pb-(hydroxy)carbonates were also identified, and their relative abundances vary dramatically between the two tailings, Fe-rich (hydroxy)sulfates being common in the Apache and rare in the Hamms, and Pb-carbonates being common in the Hamms but rare in the Apache. Pb-vanadates were detected only rarely in the Hamms tailings. Compositions of isolated Pb-phosphate and Pb-vanadate grains are consistent with Pb-bearing apatites $[(Pb,Ca)_5(PO_4,VO_4)_3(Cl,F,OH)]$ with Ca/Pb molar ratios ranging from 0 to 0.5. Analyses of Pb-carbonates in the Hamms and Pb-bearing Fe-rich sulfates in the Apache indicate that these materials are hydrous, although oxygen was not analyzed directly.

Pb L_{III}-EXAFS data shows that the majority (85%) of total Pb in the fine fraction of the Apache Tailings is accounted for by plumbojarosite $\{Pb[Fe_3(SO_4)_2(OH)_6]_2\}$ with a relatively minor (10%) contribution from plumboferrite ($PbFe_4O_7$; Holstam et al. 1995, for discussion) (Fig. 10). The identification of plumbojarosite in the

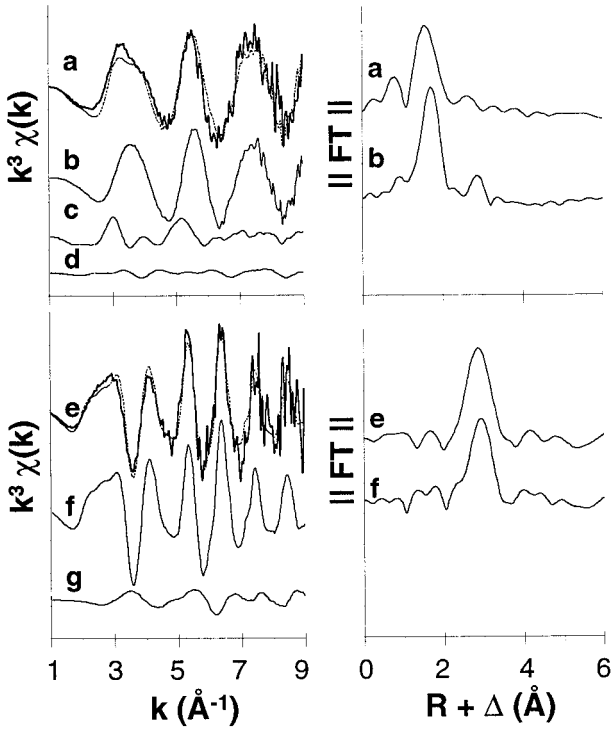

FIGURE 10. Linear least-squares fitting of the Pb L_{III}-EXAFS $k^3\chi(k)$ functions from the Leadville tailings samples showing fit components (scaled to their contributions to the fit) and RDFs for the two samples and the dominant component in each fit. (**a**) Experimental (bold line) and calculated (dashed) fit to Hamms <10 μm fraction, (**b**) 53% Pb^{2+} adsorbed on synthetic goethite, (**c**) 27% pyromorphite $[Pb_5(PO_4)_3Cl]$, (**d**) 8% hydrocerussite $[Pb_3(CO_3)_2(OH)_2]$, (**e**) experimental (bold line) and calculated (dashed) fit to Apache <5 μm fraction, (**f**) 85% plumbojarosite $\{Pb[Fe_3(SO_4)_2(OH)_6]_2\}$, and (**g**) 10% plumboferrite ($PbFe_4O_7$).

Apache sample is supported by the jarosite detection by XRD as well as the Pb-bearing Fe-rich (hydroxy)sulfates identified by EPMA. In contrast, the Hamms tailings are dominated by adsorbed Pb^{2+} (53%) with secondary contributions from pyromorphite $[Pb_5(PO_4)_3Cl]$ (27%) and hydrocerussite $[Pb_3(CO_3)_2(OH)_2]$ (8%). EXAFS data thus confirm that Pb-phosphates identified by EPMA occur as pyromorphite and are consistent with Pb-(hydroxy)carbonates occurring as hydrocerussite. While Pb-phosphates and carbonates are readily detected by EPMA in these materials, EXAFS data are essential for identifying the mode of association between Pb and Fe (hydr)oxides. Quite reasonably, Pb associated with Fe in the sulfide-rich, low-pH Apache tailings is attributable to crystalline Pb/Fe phases, whereas it is attributable mainly to Pb^{2+} adsorbed on Fe (hydr)oxides in the carbonate-rich, near-neutral pH Hamms tailings.

Results of shell fitting of the EXAFS in these samples are consistent with the primary phase identifications made by empirical fitting. The RDF of the Hamms spectrum clearly shows a dominant first-shell contribution at $R + \Delta = 1.8$ Å, which is fit by a single shell of O atoms at 2.28 Å. This distance and the relatively weak second neighbor features in this spectrum are consistent with this sample being dominated by adsorbed Pb on Fe (hydr)oxides, and a second shell of Fe can also be fit to this spectrum at 3.32 Å [consistent with Pb edge-sharing to $Fe(O,OH)_6$ octahedra] (Table 3). Additional components are, however, required to improve this fit, and were further suggested by the low coordination numbers determined by this fitting (1.6 O and 0.3 Fe) relative to those typically observed for Pb adsorbed on (hydr)oxides (e.g., 2.6 O and 0.6 Fe in the Pb sorbed on the goethite model used for this fitting; see also Bargar et al. 1997a,b).

The similarity of the Apache EXAFS spectrum with that of plumbojarosite shown by empirical fitting is also directly supported by shell fitting. As in the plumbojarosite model, the RDF of the Apache spectrum is dominated by a large contribution at $R + \Delta = 2.9$ Å (Fig. 10e). In both the plumbojarosite model and the Apache spectrum, this feature is fit by second-neighbor Fe atoms at 3.55 Å, which corresponded closely with the ideal plumbojarosite structure (6 Fe at 3.55 Å) as presented by Szymanski (1985). First-shell O atoms in the plumbojarosite structure (6 at 2.69 Å and 6 at 2.95 Å) give rise to EXAFS oscillations that are nearly out of phase with one another and, therefore, do not contribute significantly to the RDF. Furthermore, contributions from longer scattering paths (longer shell distances and/or multiple scattering) are relatively weak. As a result, although jarosites occur in a wide range of compositions (Scott 1987, for discussion), the Pb L_{III}-EXAFS of plumbojarosite should be relatively insensitive to chemical variations within the jarosite solid solution system. Thus, the large second-neighbor Fe contribution and absence of significant first-neighbor contributions in the Apache spectrum are indicative of Pb-bearing jarosite.

The Pb speciation in the two tailings piles from Leadville agree with what might be expected, given the pH difference between the two piles. In particular, Pb speciation in the low pH Apache is dominated by jarosites, which are a common weathering product in acidic environments (e.g., Alpers et al. 1989). Furthermore, the absence of adsorbed Pb in the Apache and its presence in the Hamms is consistent with the pH dependence of cation sorption to oxide mineral surfaces.

CONCLUSIONS

The combination of EXAFS analyses with complementary non-synchrotron-based compositional analyses provides detailed information on Pb speciation in complex environmental samples, not obtainable by a single technique. EXAFS spectroscopy is essential for characterizing sorbed and other sub-micrometer and/or poorly crystalline heavy metal species not amenable to analysis by other techniques. The combination of linear least-squares fitting of EXAFS data of complex multi-phase Pb-containing mixtures using model compounds with conventional shell fitting of the data provides a semi-quantitative estimate of the various chemical forms of Pb

in the complex mutli-phase mixtures studied including adsorbed Pb.

The most important result of this study is to provide direct evidence for adsorption processes in determining the fate of Pb in environmental systems. Pb^{2+} species adsorbed on hydrous iron oxides and manganese oxides represents more than half of the total Pb in samples originating from contrasting geochemical systems (mine tailings and smelter-impacted soils), and organic matter was recognized as the main sink for Pb in the organic rich smelter-impacted soil. These results are important for risk assessment and remediation design for Pb in the sites studied. In particular, the importance of sorbed Pb species at these sites suggests that a lowering of pH could release a large part of Pb in the soils and surface waters. In addition, hydrous iron and manganese oxides appear to act as efficient sinks for Pb in the systems studied and may serve as a natural barrier for the dissemination of Pb in groundwaters and plants.

Acknowledgments

This paper is dedicated to Charles (Charlie) Prewitt on the occasion of his 65th birthday and his retirement as Director of the Geophysical Laboratory. Although the subject matter of this paper may appear far afield from the many mineralogical contributions Charlie has made over the years, this work has benefited from the early contributions Charlie made in bringing mineralogists to synchrotron X-ray sources. Without such sources, this study would not have been possible. The authors are indebted to METALEUROP/Noyelles-Godault, for facilitating the access to the French site. The authors also acknowledge P. Chevallier and P. Populus for their help in micro-SXRF experiments at LURE as well as L. Galoisy and P. Sainctavit for their contributions to EXAFS experiments on French soils. In addition, thanks are extended to the SSRL staff for enabling us to be productive and efficient during our beamtime. We owe particular thanks to B. Hedman, P. DeCecco, R. Mayer, and B. Butler of the SSRL Biotechnology group for their technical assistance. The authors are indebted to M.C. Boisset for kindly providing the Pb-humate sample. This collaborative work was supported by U.S. Department of Energy grant DE-FG03-93ER14347-A007, in part by NSF grant EAR-9406490, by the cooperative CNRS-NSF research program under grants CNRS-INT-5914 and NSF-INT-9726528, and by the PROSE97 CNRS/INSU Program. This is IPGP contribution no. 1560.

References cited

Alloway, B. (1995) Heavy Metals in Soils. Blackie Academic and Professional, Glasgow, Scotland.

Alpers, C.N., Nordstrom, D.K., and Ball, J.W. (1989) Solubility of jarosite solid solutions precipitated from acid mine waters, Iron Mountain, California, U.S.A. Sciences Geologiques, Bulletin, Strasbourg, 42, 281–298.

ASARCO, Inc. (1993) Lead Speciation Study, Leadville, Colorado, U.S.A.

Bargar, J.R., Towle, S.N., Brown, G.E. Jr., and Parks, G.A. (1996) Outer-sphere lead(II) adsorbed at specific surface sites on single crystal a-alumina. Geochimica et Cosmochimica Acta, 60:3541–3547.

Bargar, J.R., Brown, G.E. Jr., and Parks, G.A. (1997a) Surface complexation of Pb(II) at oxide-water interfaces: I. XAFS and bond-valence determination of mononuclear and polynuclear Pb(II) sorption products on aluminum oxides. Geochimica et Cosmochimica Acta, 61, 2617–2637.

———(1997b) Surface complexation of Pb(II) at oxide-water interfaces: II. XAFS and bond-valence determination of mononuclear Pb(II) sorption products and surface functional groups on iron oxides. Geochimica et Cosmochimica Acta, 61, 2639–2652.

Bargar, J.R., Towle, S.N., Brown, G.E. Jr., and Parks, G.A. (1997c) XAFS and bond-valence determination of the structures and compositions of functional groups and Pb(II) and Co(II) sorption products on single-crystal α-Al_2O_3. Journal of Colloid and Interface Science, 185, 473–492.

Bargar, J.R., Brown, G.E., Jr., and Parks, G.A. (1998) Surface complexation of Pb(II) at oxide-water interfaces: III. XAFS determination of Pb(II) and Pb(II) chloro adsorption complexes on goethite and alumina. Geochimica et Cosmochimica Acta, 62, 193–207.

Boisset, M.C. (1995) étude structurale des oxydes hydratés de fer et de manganèse. Interaction avec une surface. Application au piégeage du plomb dans le milieu naturel. Ph.D. Thesis, University of Paris 6 and 7.

Bonnin, D., Calas, G., Suquet, H., and Pezerat, H. (1985) Sites occupancy of Fe^{3+} in Garfield nontronite: a spectroscopic study. Physics and Chemistry of Minerals, 12, 55–64.

Chisholm-Brause, C.J., Hayes, K.F., Roe, A.L., Brown, G.E. Jr., Parks, G.A., and Leckie, J.O. (1990) Spectroscopic investigation of Pb(II) complexes at the γ-Al_2O_3/water interface. Geochimica et Cosmochimica Acta, 54, 1897–1909.

Clevenger, T.E., Salwan, C., and Koirtyohann, S.R. (1991) Lead speciation of particles on air filters collected in the vicinity of a lead smelter. Environmental Science and Technology, 25, 1128–1133.

Cotter-Howells, J.D., Champness, P.E., Charnock, J.M., and Pattrick, R.A.D. (1994) Identification of pyromorphite in mine-waste contaminated soils by ATEM and EXAFS European Journal of Soil Science, 45, 393–402.

Davis, A., Ruby, M.V., and Bergstrom, P.D. (1992) Bioavailability of arsenic and lead in soils from the Butte, Montana, Mining District. Environmental Science and Technolology, 26, 461–468.

Davis, A., Drexler, J.W., Ruby, M.V., and Nicholson, A. (1993) Micromineralogy of mine wastes in relation to lead bioavailability, Butte, Montana. Environmental Science and Technolology, 27, 1415–1425.

Farquhar, M.L., Vaughan, D.J., Hughes, C.R., Charnock, J.M., and England, K.E.R. (1997) Experimental studies of the interaction of aqueous metal cations with mineral substrates: Lead, cadmium, and copper with perthitic feldpar, muscovite, and biotite. Geochimica et Cosmochimica Acta, 61, 3051–3064.

George, G. and Pickering, I.J. (1993) EXAFSPAK. Stanford Synchrotron Radiation Laboratory. http://ssrl01.slac.stanford.edu/exafs pak.html.

Godin, P., Feinberg, M., and Ducauze, C. (1985) Modeling of soil contamination by airborne lead and cadmium around several emission sources. Environmental Pollution Series B, 10, 97–114.

Gulson, B.L., Mizon, K.J., Law, A.J., Korsch, M.J., Davis, J.J., and Howarth, D. (1994) Source and pathways of lead in humans from the Broken Hill Mining Community—an alternative use of exploration methods. Economic Geology, 89, 889–908.

Holstam, D., Norrestam, R., and Sjodin, A. (1995) Plumboferrite: new mineralogical data and atomic arrangement. American Mineralogist, 80, 1065–1072.

Kimball, B.A., Callender, E., and Axtmann, E.V. (1995) Effects of colloids on metal transport in a river receiving acid mine drainage, upper Arkansas River, Colorado, U.S.A. Applied Geochemistry, 10, 285–306.

Kinniburgh, D.G., Milne, C.J., Benedetti, M.F., Pinheiro, J.P., Filius, J., Koopal, L.K., and Van Riemsdijk, W.H. (1996) Metal ion binding by humic acid: application of the NICA-Donnan model. Environmental Science and Technolology, 30, 1687–1698.

Krauskopf, K.B. (1992) Environmental Geochemistry. In Encyclopedia of Physical Science and Technology, Vol. 6, p. 185–214. Academic Press, New York.

Levy, D.B., Barbarick, E.G., Siemer, E.G., and Sommers, L.E. (1992) Distribution and partitioning of trace metals in contaminated soils near Leadville, Colorado. Journal of Environmental Quality, 21, 185–195.

Manceau, A., Charlet, L., Boisset, M.C., Didier, B., and Spadini, L. (1992) Sorption and speciation of heavy metals on hydrous Fe and Mn oxides: from microscopic to macroscopic. Applied Clay Science, 7, 201–223.

Manceau, A., Boisset, M.C., Sarret, G., Hazemann, J.L., Mench, M., Cambier, P., and Prost, R. (1996) Direct determination of lead speciation in contaminated soils by EXAFS spectroscopy. Environmental Science and Technolology, 30, 1540–1552.

Ministère de l'Environnment (1996) Recensement 1996 des sites et sols pollués, Published by the Ministère de l'Aménagement du Territoire et de l'Environnment, France.

Miller, W.P., Martens, D.C., and Zelazny, L.W. (1986) Effect of sequence in extraction of trace metals from soils. Soil Science Society of America Journal, 50, 598–601.

Moore, P.B., Gupta, P.K.S, and Le Page, Y. (1989) Magnetoplumbite, $Pb^{2+}Fe^{2+}_{12}O_{19}$: refinement and lone-pair splitting. American Mineralogist, 74, 1186–1194.

O'Day, P.A., Rehr, J.J., Zabinsky, S.I., and Brown, G.E. Jr. (1994) Extended X-ray Absorption Fine Structure (EXAFS) analysis of disorder and multiple-scattering in complex crystalline solids. Journal of the American Chemical Society, 116, 2938–2949.

O'Day, P.A., Carroll, S.A., and Waychunas, G.A. (1998) Rock-water interactions controlling zinc, cadmium, and lead concentrations in surface waters and sediments, U.S. Tri-State Mining District 1. Molecular identification using X-ray absorption spectroscopy. Environmental Science and Technolology, 32, 943–955.

Post, E. and Bish, D.L. (1989) Rietveld refinement of the coronadite structure. American Mineralogist, 74, 913–917.

Roe, A.L., Hayes, K.F., Chisholm-Brause, C.J., Brown, G.E. Jr., Parks, G.A., Hodgson, K.O., and Leckie, J.O. (1991) In situ X-ray absorption study of lead ion surface complexes at the goethite-water interface. Langmuir, 7, 367–373.

Ruby, M.V., Davis, A., Kempton, J.H., Drexler, J.W., and Bergstrom, P.D. (1992) Lead bioavailability: dissolution kinetics under simulated gastric conditions. Environmental Science and Technolology, 26, 1242–1248.

Scott, K.M. (1987) Solid solution in and classification of gossan-derived members of the alunite-jarosite family, Northwest Queensland, Australia. American Mineralogist, 72, 178–187.

Szymanski, J. (1985) The crystal structure of plumbojarosite $Pb[Fe_3(SO_4)_2(OH)_6]_2$. Canadian Mineralogist, 23, 659–668.

Tessier, A., Fortin, D., Belize, N., DeVitre, R.R., and Leppard, G.G. (1996) Metal sorption to diagenetic iron and manganese oxyhydroxides and associated organic matter: narrowing the gap between field and laboratory measurements. Geochimica et Cosmochimica Acta, 60, 387–404.

Xia, K., Bleam, W., and Helmke, P.A. (1997) Studies of the nature of Cu^{2+} and Pb^{2+} binding sites in soil humic substances using X-ray absorption spectroscopy. Geochimica et Cosmochimica Acta, 61, 2211–2221.

Zabinsky, S.I., Rehr, J.J., Ankudinov, A., Albers, R.C., and Eller, M.J. (1995) Multiple-scattering calculations of X-ray absorption spectra. Physical Review B, 52, 2995–3009.

Manuscript received July 6, 1998
Manuscript accepted October 7, 1998
Paper handled by John Parise